Biochimica et Biophysica Acta 1844 (2014) 1486–1492

Contents lists available at ScienceDirect

Biochimica et Biophysica Acta

journal homepage: www.elsevier.com/locate/bbapap

Structural insights into the cofactor-assisted substrate recognition of yeast methylglyoxal/isovaleraldehyde reductase Gre2

Peng-Chao Guo [a,b], Zhang-Zhi Bao [b], Xiao-Xiao Ma [b], Qingyou Xia [a], Wei-Fang Li [b,*]

[a] State Key Laboratory of Silkworm Genome Biology, Southwest University, 216, Tiansheng Road, Beibei, Chongqing 400716, People's Republic of China
[b] Hefei National Laboratory for Physical Sciences at Microscale and School of Life Sciences, University of Science and Technology of China, Hefei, Anhui 230027, People's Republic of China

ARTICLE INFO

Article history:
Received 24 March 2014
Received in revised form 6 May 2014
Accepted 19 May 2014
Available online 27 May 2014

Keywords:
Methylglyoxal/isovaleraldehyde reductase
Saccharomyces cerevisiae
Crystal structure
Substrate-binding pocket
Enzymatic kinetics

ABSTRACT

Saccharomyces cerevisiae Gre2 (*EC1.1.1.283*) serves as a versatile enzyme that catalyzes the stereoselective reduction of a broad range of substrates including aliphatic and aromatic ketones, diketones, as well as aldehydes, using NADPH as the cofactor. Here we present the crystal structures of Gre2 from *S. cerevisiae* in an apo-form at 2.00 Å and NADPH-complexed form at 2.40 Å resolution. Gre2 forms a homodimer, each subunit of which contains an N-terminal Rossmann-fold domain and a variable C-terminal domain, which participates in substrate recognition. The induced fit upon binding to the cofactor NADPH makes the two domains shift toward each other, producing an interdomain cleft that better fits the substrate. Computational simulation combined with site-directed mutagenesis and enzymatic activity analysis enabled us to define a potential substrate-binding pocket that determines the stringent substrate stereoselectivity for catalysis.

1. Introduction

Keto-aldehydes, such as methylglyoxal, are associated with a broad spectrum of biological effects, including regulation of the cell cycle in diverse organisms, microtubule assembly, inhibition of protein synthesis, and carcinogenicity. Thus, cellular accumulation of methylglyoxal leads to serious cytostatic and cytotoxic effects [1]. To eliminate toxic methylglyoxal, organisms have evolved to produce diverse enzymes that catalyze the NADPH-dependent reduction of a variety of carbonyl compounds in microorganisms, mammals and plants. For instance, methylglyoxal reductases protect cells from the cytotoxic effects of methylglyoxal by the reduction of methylglyoxal to lactaldehyde, using either NADH or NADPH as an electron donor [2].

NADPH-dependent methylglyoxal reductases (*EC1.1.1.283*) belong to the short-chain dehydrogenase/reductase (SDR) superfamily [3], which includes various oxidoreductases, some isomerases and lyases [4,5]. Despite the low sequence identity (15–30%) of these SDR enzymes, they adopt a quite similar fold, except in the substrate binding cleft [6]. The SDR enzymes have a characteristic Rossmann fold for cofactor binding and a relatively conserved "Ser-Tyr-Lys" ("Ala-Tyr-Lys" in dihydropteridine reductase from rat liver) catalytic triad [5,7]. However, there is considerable variation in the form of substrate binding clefts, which consists of the wide substrate spectrum of this enzyme superfamily [8].

The NADPH-dependent methylglyoxal reductase in *Saccharomyces cerevisiae* was termed Gre2 (genes de respuesta a estres, Spanish, meaning "stress-responsive gene"), for the expression of the *GRE2* gene is often induced by stress conditions, including osmotic, ionic, oxidative, heat shock, and heavy metal related stress [9–13]. In addition to the reduction of methylglyoxal, Gre2 could act as a suppressor of filamentation by virtue of encoding isovaleraldehyde reductase activity *in vivo* [14,15]. Thus, Gre2 was subsequently annotated as isovaleraldehyde reductase beyond the methylglyoxal reductase. Similar to other SDR enzymes, Gre2 could also catalyze the reduction of not only diketones, but also aliphatic and cyclic α- and β-keto esters and aldehydes, as well as ketones [3]. Moreover, Gre2 is a highly valuable biocatalyst that catalyzes a wide variety of carbonyl compounds (ketones, diketones and ketoesters) to chiral molecules, which are necessary building blocks in the pharmaceutical industry. This includes the stereoselective biosynthesis of (2S, 5S)-hexanediol by the reduction of 2,5-hexanedione [3,16] and the biosynthesis (S)-3-chloro-1-phenyl-propanol by the reduction of 3-chloro-1-phenyl-propanone [17].

Although a preliminary X-ray structural analysis of Gre2 has been reported [18], little is known about the substrate recognition and the catalytic mechanism underlying the stereoselective reduction of Gre2. Here, we determined the crystal structures of Gre2, in the apo-form at 2.00 Å and NADPH-complexed form at 2.40 Å. The structures enabled us to identify a noticeable induced fit upon NADPH binding. We also defined a substrate-binding site using computational simulation and enzymatic activity assays.

* Corresponding author. Tel.: +86 551 63600406.
E-mail address: liwf@ustc.edu.cn (W.-F. Li).

http://dx.doi.org/10.1016/j.bbapap.2014.05.008
1570-9639/

2. Materials and methods

2.1. Overexpression and purification of Gre2 and mutants

The coding sequence of *GRE2/YOL151W* was amplified by PCR, using *S. cerevisiae* S288c genomic DNA as the template, and cloned into a pET28a-derived vector. This construct adds a hexahistidine-tag to the N-terminus of the recombinant protein, which was over-expressed in an *E. coli* BL21 (DE3) (Novagen, Madison, WI) strain using a 2 × YT culture medium. The cells were induced with 0.2 mM isopropyl-β-D-thiogalactoside (IPTG) at 16 °C for 20 h when OD_{600nm} reached 0.6. Cells were harvested by centrifugation at 8000 *g* for 10 min and resuspended in lysis buffer (20 mM Tris–HCl, pH 7.0, and 200 mM NaCl). After 5 min of sonication and centrifugation at 12,000 *g* for 25 min, the supernatant containing the soluble target protein was collected and loaded to a Ni-NTA column (GE Healthcare) equilibrated with binding buffer (20 mM Tris–HCl, pH 7.0, and 200 mM NaCl). The target protein was eluted with 250 mM imidazole buffer and further loaded onto a Superdex 75 column (GE Healthcare) equilibrated with 20 mM Tris–HCl, pH 7.0, and 50 mM NaCl. Fractions containing the target protein were pooled and concentrated to 20 mg/mL by ultrafiltration (Millipore, 10 kDa cut-off). The purity of the protein was estimated on SDS-PAGE and the protein sample was stored at −80 °C. The mutant proteins were expressed, purified, and stored in the same manner as the wild-type protein.

2.2. Crystallization, data collection, structure solution, and refinement

Crystals of Gre2 were obtained at 289 K using the hanging drop vapor-diffusion techniques, with the initial condition of mixing 1 μL of the 20 mg/mL protein sample with an equal volume of mother liquor (25% polyethylene glycol 2000 MME, 0.2 M $(NH_4)_2SO_4$, and 0.1 M sodium acetate, pH 4.6). The crystals grew to approximately 0.1 × 0.2 × 0.4 mm in about 3 days. Crystals of the Gre2–NADPH complex were obtained by co-crystallizing Gre2 with 5 mM NADPH in the same mother liquor. The crystals were transferred to a cryoprotectant [reservoir solution supplemented with 25% (v/v) glycerol] and flash-cooled at 100 K in liquid nitrogen. Both data were collected at a radiation wavelength of 0.9795 Å at the Shanghai Synchrotron Radiation Facility, Shanghai Institute of Applied Physics, Chinese Academy of Sciences, using a beamline BL17U at 100 K with a Q315r CCD (Marresearch). Data processing and scaling were performed using the HKL2000 package [19]. Both crystal structures were determined by the molecular replacement method with *MOLREP* [20] using the coordinates of *Sporobolomyces salmonicolor* aldehyde reductase (PDB ID: 1Y1P, sequence identity is 30%) as the search model. Refinement was carried out using *REFMAC* [21] and *Coot* [22]. The overall assessment of model quality was performed using *MolProbity* [23]. The crystallographic parameters of the structures are listed in Table 1. All structural figures were prepared with *PyMOL* [24].

Table 1
Data-collection statistics for the crystal of yeast Gre2 and the Gre2–NADPH complex.

	Gre2	Gre2–NADPH complex
Data collection		
Space group	*P*212121	*P*212121
Unit cell (Å, °)	48.72, 97.85, 139.00	
90, 90, 90	90.31, 92.89, 201.09	
90, 90, 90		
Molecules per asymmetric unit	2	4
Resolution range (Å)[a]	50.00–2.00 (2.03–2.00)	50.00–2.40 (2.44–2.40)
Unique reflections	45,207 (22,08)	67,436 (3,332)
Completeness (%)	99.2 (97.1)	99.3 (100.0)
<I/σ(I)>	18.07 (6.32)	15.93 (3.52)
R_{merge}[b] (%)	7.9 (20.7)	8.9 (46.3)
Average redundancy	4.5 (4.0)	5.6 (5.7)
Structure refinement		
Resolution range (Å)	50.00–2.00	
(2.05–2.00)	50.00–2.40	
(2.46–2.40)		
R-factor[c]/R-free[d] (%)	22.4/26.6	24.2/28.8
Number of protein atoms	5380	10194
Number of water atoms	346	128
RMSD[e] bond lengths (Å)	0.008	0.007
RMSD bond angles (°)	1.044	1.105
Mean B factors (Å^2)	56.9	50.9
Ramachandran plot[f]		
Most favored (%)	98.4	98.3
Additional allowed (%)	1.2	1.3
PDB ID	4PVC	4PVD

[a] Values in parentheses are for the highest resolution shell.
[b] $R_{merge} = \sum_{hkl}\sum_i|I_i(hkl) - \langle I(hkl)\rangle| / \sum_{hkl}\sum_i|I_i(hkl)|$, where $I_i(hkl)$ is the intensity of an observation and $\langle I(hkl)\rangle$ is the mean value for its unique reflection; summations are over all reflections.
[c] R-factor $= \sum_h||Fo(h)| - |Fc(h)|| / \sum_h|Fo(h)|$, where Fo and Fc are the observed and calculated structure-factor amplitudes, respectively.
[d] R-free was calculated with 5% of the data excluded from the refinement.
[e] Root-mean square-deviation from ideal values.
[f] Categories as defined by *MolProbity*.

2.3. Computational docking

The three dimensional structure of isovaleraldehyde was transformed with the program phniex.elbow [25] from the simplified molecular input line entry specification (SMILES) level representations CC(C)CC=O. Docking runs were performed using the program HADDOCK [26], based on our Gre2–NADPH structure. Up to 15 initial clusters were generated, for each of which multiple conformations were scored. The best scoring pose was a rigid-body minimized and scored for electrostatic and van der Waals interactions.

2.4. Enzymatic activity assay

The kinetic parameters of native Gre2 and its mutants were measured as previously described [17] with minor changes. All assays were performed at 30 °C in a standard assay mixture containing 100 mM phosphate buffer, pH 7.5, 0.2 mM NADPH, purified protein and substrates at various concentrations. Isovaleraldehyde was dissolved in absolute alcohol (final concentration of alcohol in assay was 1%). The reactions were triggered by adding the purified protein solution, and the decrease in absorbance at 340 nm ($\varepsilon_{NADPH} = 6220\ M^{-1}\ cm^{-1}$) was monitored with a DU800 spectrophotometer (Beckman Coulter) equipped with a cuvette holder fixed at 30 °C. The decrease of absorbance resulting from the non-enzymatic reduction of substrates upon addition of NADPH was set as background control for each assay.

3. Results and discussion

3.1. Overall structure

An asymmetric unit of Gre2 contains two subunits, with an overall root mean square deviation (RMSD) of 0.26 Å over 316 Cα atoms (Fig. S1A). The two subunits have a buried interface of 1050 Å^2 that might be due to the crystal packing, because the result of *PISA* [27] evaluation and the analysis of gel filtration chromatography demonstrated that Gre2 was monomeric (Fig. S1B). A Gre2 molecule can be divided into two distinct domains: an N-terminal cofactor-binding domain and a C-terminal substrate-binding domain (Fig. 1A). The cofactor-binding domain adopts a Rossmann-fold motif [28], with a parallel seven-stranded-sheet sandwiched by a total of six-helices (α1–5, and α7). Notably, the dinucleotide-binding motif ($G_7A_8N_9G_{10}F_{11}I_{12}A_{13}$) locates at the region between β1 and α1. The substrate-binding domain has four α-helices (α6 and α8–10) and one twisted β-sheet, formed by β1′, β2′, and β3′, located so as to cover the bound NADPH.

A Dali protein structural similarity search (http://ekhidna.biocenter.helsinki.fi/dali_server/) revealed that Gre2 is structurally similar with

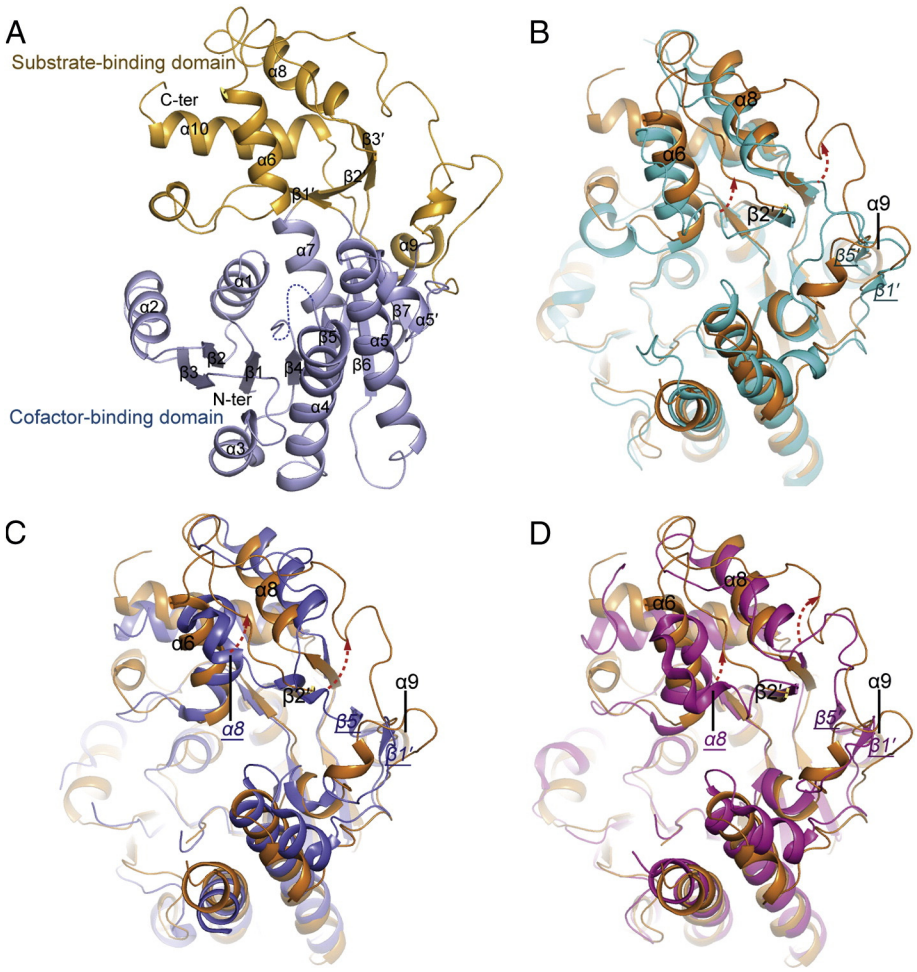

Fig. 1. Overall structure. (A) Cartoon representation of the Gre2 molecular structure. Blue, N-terminal domain; orange, C-terminal domain. (B) Comparison of the overall structure between Gre2 (orange) and *Ss*AR (PDB ID: 1ZZE, cyan), (C) *Ms*VR (PDB ID: 2P4H, blue) and (D) *Vv*DFR (PDB ID: 3C1T, light magenta). All figures were prepared using *PyMOL*. The secondary structure elements of Gre2 and the counterparts of SDR proteins are marked with black roman and color italics, respectively.

several SDR enzymes, such as, *Sporobolomyces salmonicolor* aldehyde reductase (*Ss*AR, PDB ID: 1ZZE), *Medicago sativa* L. vestitone reductase (*Ms*VR, PDB ID: 2P4H) and *Vitis vinifera* dihydroflavonol 4-reductase (*Vv*DFR, PDB ID: 3C1T). Superposition of Gre2 against these structures yields an overall RMSD in the range of 2.6–3.0 Å over approximately 240 Cα atoms. Structural comparison suggests that Gre2 and all SDR enzymes adopt a quite similar pattern of Rossmann fold in the cofactor-binding domain. Nevertheless, the major differences between Gre2 and these counterparts are in their C-terminal domain (Fig. 1B, C and D). Notably, the counterpart of the small β-sheet (formed by *β1′* and *β5′*) in *Ss*AR, *Ms*VR and *Vv*DFR is flexible loops in Gre2, whereas the counterpart of a small helix (*α8*, Gly216–Ile221, residue numbering corresponds to *Ms*VR) in the *Ms*VR and *Vv*DFR is a loop (between α6 and β2′) in the Gre2 structure. Furthermore, the segment between α6 and β2′ and the loop region between α8 and α9 in Gre2 are away from the cofactor-binding cleft, as compared to that of the counterparts of SDR proteins [29–31].

3.2. Induced fit upon NADPH-binding

In the NADPH-complexed Gre2, one NADPH binds to the cleft between the N- and C-terminal domains (Fig. 2A), and interacts with residues from both domains (Fig. 2B). The NADPH adenine ring is sandwiched between the main chains of Ser83 and Pro84 and the side chains of Arg32 and Ile58 *via* van der Waal's contacts. The amino group of the adenine moiety is bound by a hydrogen bond with Asp57-Oδ2. As expected, the residues Gly7–Ala13 of the dinucleotide-binding motif mainly interact with the ribose of adenosine and diphosphate moiety *via* five hydrogen bonds. In details, the hydroxyl group of the adenosine ribose forms two hydrogen bonds with Gly7-O and Gly10-N. The phosphate moiety of adenosine form hydrogen bonds with Asn9-Nδ2, Arg32-Nη and Lys36-Nζ, giving Gre2 a stronger affinity for NADPH than NADH. The diphosphate fits into the relatively narrower part of the cleft, and forms hydrogen bonds with the main-chain atoms of Phe11 and Ile12. The two hydroxyl groups of the nicotinamide ribose are stabilized by Tyr165-Oη and Lys169-Nζ *via* two hydrogen bonds. The nicotinamide moiety fits into a wider cavity and makes two hydrogen bonds with Val199-N and Ser216-Oγ (Fig. 2B).

The superposition of the apo form against the NADPH-complexed Gre2 yields an RMSD of 0.7 Å over 309 Cα atoms, and reveals a conformational change induced by NADPH binding. Upon the binding of NADPH, the helix α4 in the cofactor-binding domain rotated toward the NADPH at an angle of 8.5° along its C-terminus. Furthermore, the helices α5′, α5 and α6 also rigidly shift toward NADPH (Fig. 2C). In addition, the loop region (Pro84–Cys86) between β4 and α5 is bent to the diphosphate group and packs against NADPH, whereas this segment is not visible in the 2Fo–Fc electron density map of the apo form, presumably due to its high flexibility. These conformational changes lead to a narrower interdomain cleft for the approaching NADPH molecule (Fig. 2D). The side chains of Arg32, Asp57 and Ile58 shift about 2.0, 1.5 and 1.2 Å, respectively, toward the adenosine ring of NADPH. The residues Ser83 and Pro84 shift about 0.9 and 4.1 Å toward the diphosphate group, leaving space for the accommodation of the

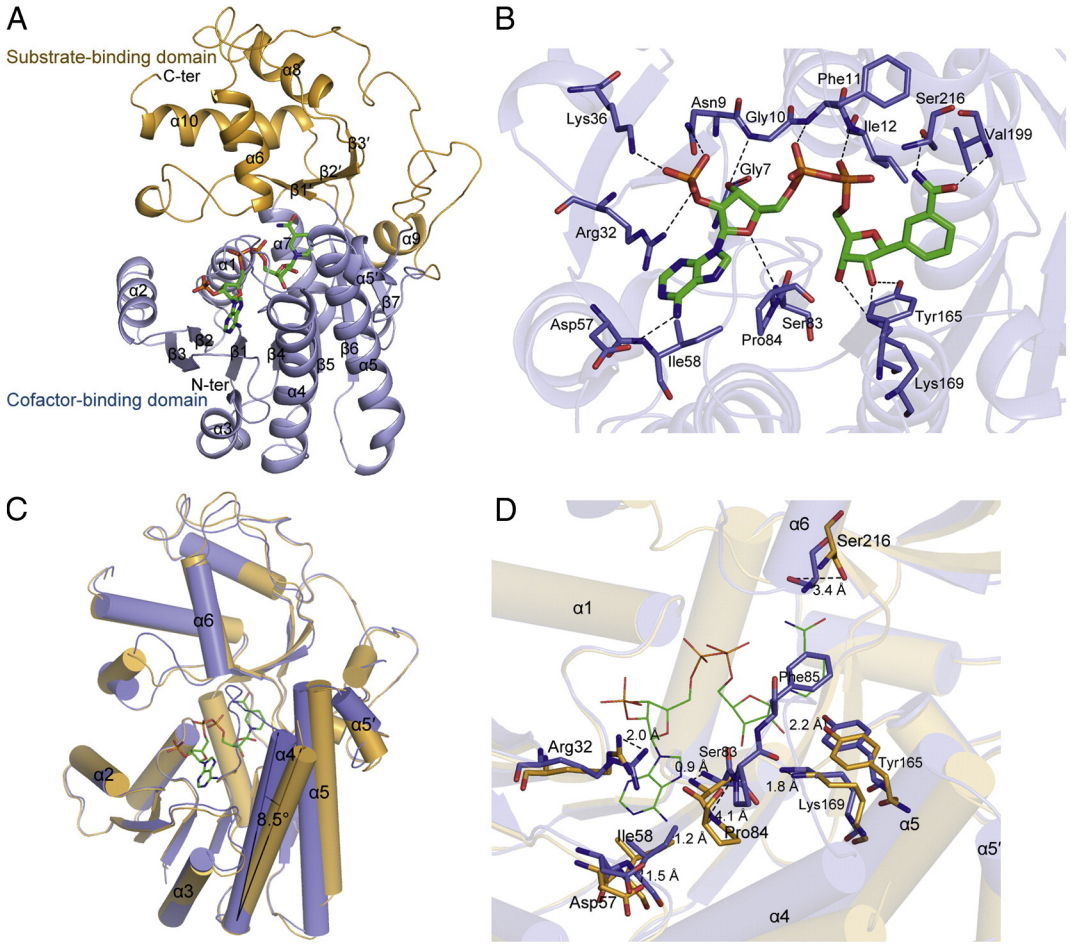

Fig. 2. NADPH binding. (A) Cartoon representation of the Gre2–NADPH complex monomer. (B) Hydrogen bonds between NADPH and surrounding residues are black dashed lines. Residues are shown in blue stick format, NADPH is green. Comparison of (C) the overall structure and (D) the residues in the cofactor-binding pocket between apo-Gre2 and the Gre2–NADPH complex; orange, Gre2; blue, Gre2–NADPH complex; green, NADPH.

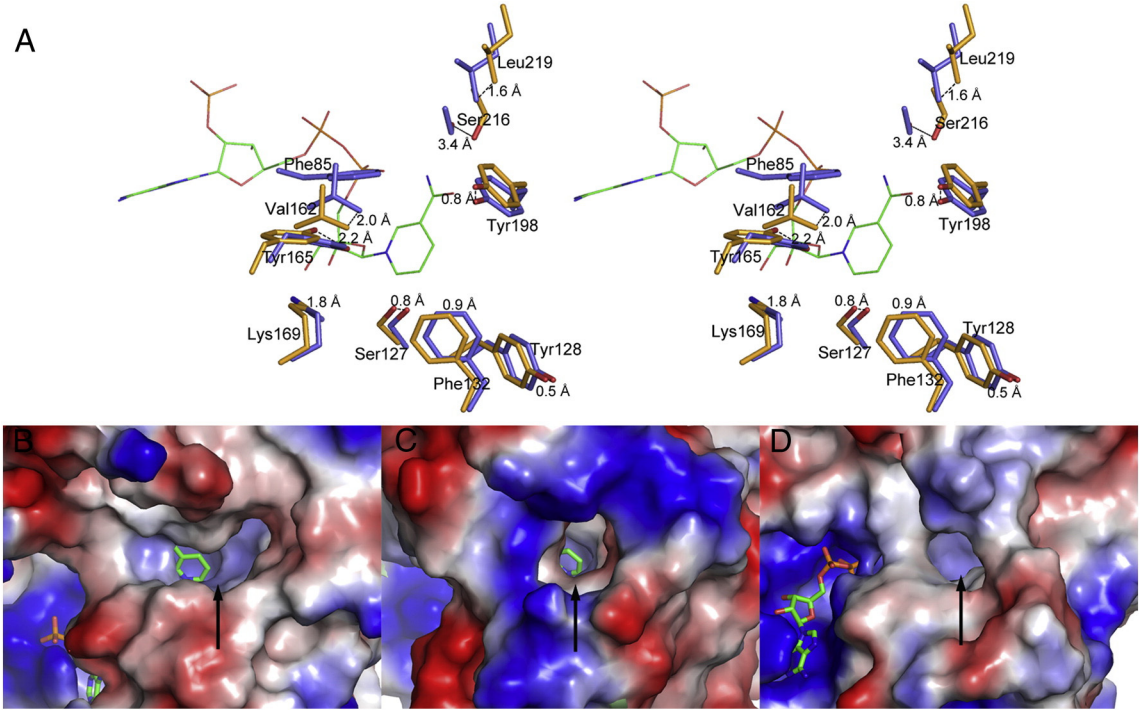

Fig. 3. Substrate-binding pocket. (A) Stereoview of the superposition of residues in the substrate-binding pocket. Orange, Gre2; blue, Gre2–NADPH complex; green, NADPH. The size of the substrate-binding pocket of (B) Gre2, (C) *Ss*AR (PDB ID: 1Y1P) and (D) *Vv*DFR (PDB ID: 2C29). The position of the pockets was marked with black arrows.

NADPH adenine moiety. The side chains of Tyr165, Lys169 and Ser216 also shifted about 2.2, 1.8 and 3.4 Å to stabilize the nicotinamide moiety of NADPH (Fig. 2D).

Upon NADPH binding, the conformational change in Gre2 is consistent with that of liver alcohol dehydrogenases [32,33] and quinone reductase [34], which result in a narrowing of the cofactor-binding clefts, and the active sites are shielded from the solvent (Fig. 2B). However, in the NADPH-complexed *Ss*AR (PDB ID: 1ZZE/1Y1P), no obvious conformational changes are found around the NADPH-binding cleft [29].

3.3. Substrate-binding pocket

In addition to the residues Phe85, Tyr165, Lys169 and Ser216 shifting toward the nicotinamide moiety of NADPH (Figs. 2D and 3A), there are several other residues located near the C4 atom of the nicotinamide ring undergoing significant conformational changes upon NADPH binding (Fig. 3A). For example, the main chains of Val162 and Leu219 shift toward the nicotinamide ring, together with the side chains reorienting by 2.0 and 1.6 Å, respectively. The side chains of Ser127, Tyr128, Phe132 and Tyr198 are shifted about 0.8, 0.5, 0.9 and 0.8 Å, respectively. These residues, together with the nicotinamide ring, form a substrate-binding pocket, as proposed previously [17]. The aromatic residues (Phe85, Tyr128, Phe132, Tyr165 and Tyr198) and hydrophobic residues (Val162 and Leu219) formed the hydrophobic sidewall of the pocket. The hydrophilic residues Ser127, Lys169 and Ser216, together with the nicotinamide ring formed the bottom of the pocket. Moreover, a conserved Ser-Tyr-Lys triad was identified for the catalytic mechanisms of the SDR enzymes [5]. In the Gre2 structure, the conserved $Y_{165}XXXK_{169}$ motif is located near the C4 atom of the nicotinamide ring, and Ser127 is located in the position corresponding to the serine of the catalytic triad of SDR enzymes. Thus, Ser127, together with Tyr165 and Lys169, may act as the catalytic triad for Gre2 (Fig. 3A).

Structural comparison revealed that the substrate-binding pocket in Gre2–NADPH is relatively extended (Fig. 3B) compared to *Ss*AR–NADPH (PDB ID: 1Y1P) (Fig. 3C) and *Vv*DFR–NADPH (PDB ID: 2C29) (Fig. 3D). The substrate-binding pocket in Gre2 presents a funneled structure that consists of one broad pocket entrance and one deep hydrophobic channel, whereas the substrate-binding pocket in *Ss*AR and *Vv*DFR shows a relatively narrow channel. Furthermore, the funneled substrate-binding pocket of Gre2 is necessary to accommodate a wide variety of carbonyl compounds [3].

3.4. Putative binding sites of isovaleraldehyde in the substrate-binding pocket

To further explore the substrate binding pattern, we docked one physiological substrate, isovaleraldehyde, to the Gre2–NADPH complex using the program HADDOCK [26]. In the modeling process, we fixed the residues Ser127, Tyr165 and Lys169 which make up the catalytic triad to ensure that the substrate intermediate lay in a relatively reasonable pocket. Among the 15 output clusters, the cluster of lowest energy with 12 members satisfied the best interaction restraints. The overall backbone RMSD of 0.3 ± 0.2 Å for the 12 members indicated that the model is somewhat reliable. In the model, the carbonyl group of isovaleraldehyde points toward Ser127 and Tyr165, and the backbone is surrounded by aromatic residues Phe85, Tyr128, Phe132, Tyr165 and Tyr198, and the hydrophobic residue Val162 (Fig. 4A). To verify the docking results, we performed a series of site-directed mutagenesis and tested the enzymatic activity.

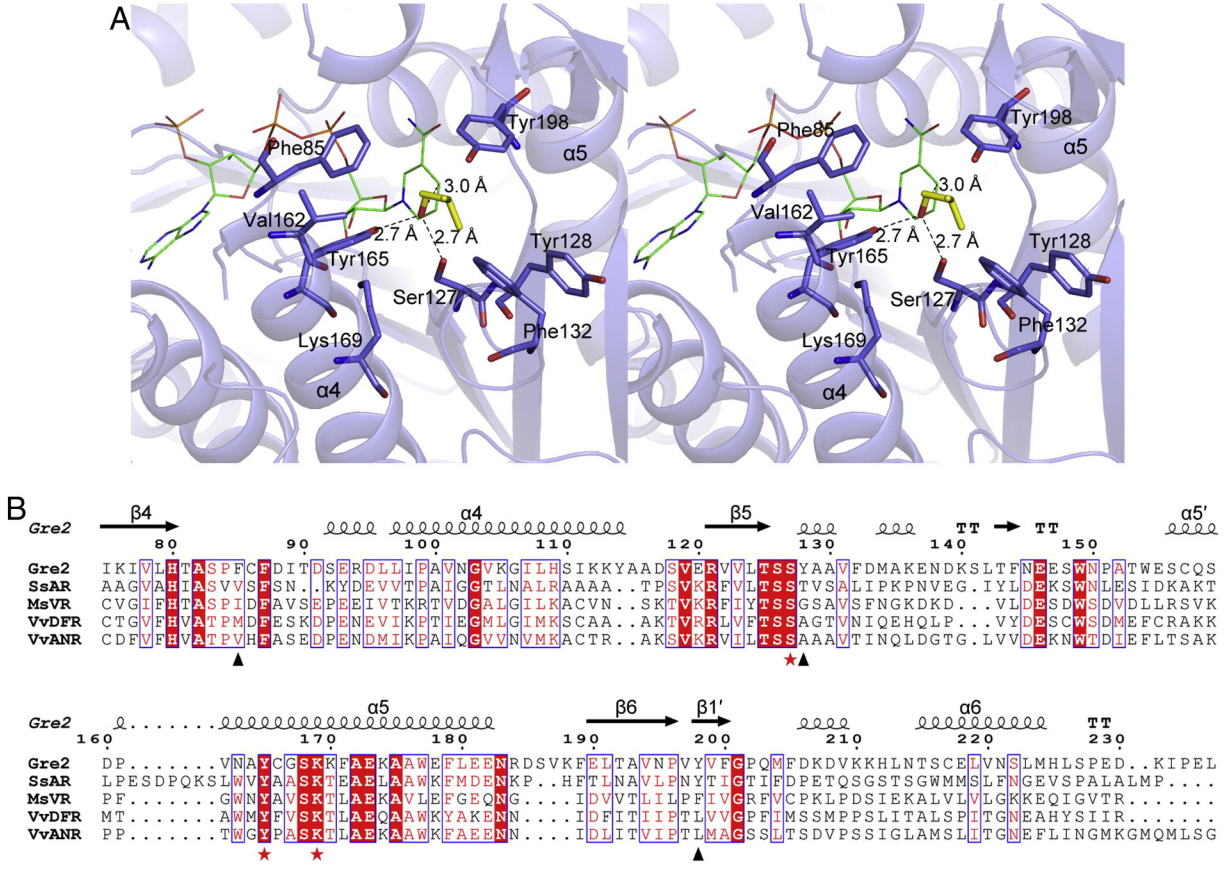

Fig. 4. Simulation and validation of the substrate-binding mode. (A) Stereoview of the isovaleraldehyde binding to the Gre2 active site. Residues are shown in blue stick format. NADPH is green, and docked isovaleraldehyde is yellow. Hydrogen bonds between the residues and docked substrate are black dashes. (B) Multiple sequence alignment of *Saccharomyces cerevisiae* Gre2 (NP_014490.1); *Ss*AR (Q9UUN9.3); *Ms*VR (Q40316.1); *Vv*DFR (NP_001268144.1) and *Vv*ANR (NP_001267885.1). Secondary structure elements of Gre2 are at the top. The catalytic triad is marked with red stars, and the residues involved in the substrate-binding are marked with black triangles. Alignments were performed with *ClustalW* [36] and *ESPript* [37].

Table 2
Kinetic parameters of the wild-type Gre2 and mutants. Activities were determined in 100 mM phosphate buffer, pH 7.5, with 0.2 mM NADPH, at 30 °C.

Isovaleraldehyde			
Enzyme	K_m (mM)	k_{cat} (S^{-1})	k_{cat}/K_m (mM^{-1} S^{-1})
Wild-type	0.14 ± 0.03	23.18 ± 1.66	160.97 ± 11.53
S127A	ND	ND	ND
Y165A	ND	ND	ND
Y165F	ND	ND	ND
K169L	ND	ND	ND
F85A	11.12 ± 3.41	5.94 ± 0.89	0.53 ± 0.08
Y128A	0.67 ± 0.22	1.44 ± 0.18	2.14 ± 0.27
Y128F	0.23 ± 0.06	38.98 ± 2.72	166.58 ± 11.62
F132A	0.18 ± 0.03	62.41 ± 2.19	342.72 ± 12.03
V162A	0.20 ± 0.04	52.57 ± 2.49	261.54 ± 12.39
Y198A	4.10 ± 0.98	9.29 ± 0.92	2.27 ± 0.22
Y198F	0.12 ± 0.04	15.53 ± 1.43	126.26 ± 11.62

The mutants of S127A, Y165A, Y165F and K169L lose all catalytic activity toward isovaleraldehyde (Table 2), suggesting the crucial roles of Ser127, Tyr165 and Lys169 in Gre2 catalysis. Similar to other SDR enzymes, the Tyr165 in Gre2 is considered to act as a catalytic base, whereas Ser127 stabilizes the substrate and the Lys169 lowers the p*Ka* value (usually about 10) of the Tyr-OH to facilitate catalysis at neutral pH [35]. We next measured the activities of the mutants of Phe85, Tyr128, Phe132, Val162 and Tyr198 (Table 2). Compared to the wild-type Gre2, the K_m values for the F85A, Y128A and Y198A mutants toward isovaleraldehyde were increased to about 77-fold, 5-fold and 28-fold, respectively, while the K_m values for Y128F and Y198F were comparable to that of the wild-type. Moreover, the k_{cat} values of mutants F85A, Y128A and Y198A toward isovaleraldehyde decreased by 6–40% compared to that of the wild-type. These results indicated that residues Phe85, Tyr128, and Tyr198 are involved in substrate binding and positioning *via* hydrophobic interactions. As observed in the structure of Gre2, Phe85, Tyr128 and Tyr128 shaping a hydrophobic environment around the C4 atom of NADPH facilitates electron transfer. It is worthy to notice that, the K_m value for F132A and V162A toward isovaleraldehyde showed little change, whereas, the k_{cat} and k_{cat}/K_m values of F132A and V162A increased about 2–3 fold, implying that residues Phe132 and Val162 are only involved in forming the entrance of a substrate-binding pocket, but not immobilizing the isovaleraldehyde. Thus, the replacement of Phe132/Val162, with Ala resulted in the elevation of enzymatic activity toward isovaleraldehyde, probably *via* enlarging the pocket entrance.

Taken together, these results indicated that the docking mode probably resembles the natural binding of the isovaleraldehyde (Fig. 4A): the carbonyl oxygen interacts with the side chain of Ser127, Tyr165 through hydrogen bonds (about 2.7 Å), giving a distance of 3.0 Å between the C4 atom of the nicotinamide and the carbonyl carbon of substrate. The $(CH_3)_2CHCH_2-C=$ group of isovaleraldehyde, is identified and stabilized by this hydrophobic channel *via* hydrophobic interactions. Thus, we deduced that the re-distribution of hydrophobic and polar residues in the pocket upon NADPH binding creates an ideal environment for accommodating both the hydrophobic and polar moieties of the substrates. Furthermore, multiple-sequence alignment shows that the residues of the catalytic triad Ser127, Tyr165 and Lys169 are highly conserved in the Gre2 homologues, and essential for enzyme catalysis and function. The Phe85, Tyr128 and Tyr198 residues that formed hydrophobic interactions with substrate are relatively conserved (Fig. 4B). In Gre2, these hydrophobic residues combined with Phe132 and Val162 to form one funneled pocket which consists of one broad pocket entrance and one deep hydrophobic channel. The extended hydrophobic entrance of Gre2 plays a role in accommodating a wide variety of carbonyl compounds, such as diketones, aliphatic and cyclic α- and β-keto esters and aldehydes [3]. However, the deep hydrophobic channel prefers to identify a substrate with a liner substrate. That is why Gre2 shows high reduction activity to butanal, pentanal and 2,5-hexanedione, as well as some aldehydes [3].

3.5. Putative mechanism for catalysis

The present structures and the previous reports [35] enabled us to propose the putative catalytic mechanism of Gre2 (Fig. 5): in the first step, the hydroxyl groups of the Ser127 and Tyr165 residues form hydrogen bonds with the carbonyl oxygen of isovaleraldehyde, stabilizing its position. Subsequently, the hydroxyl group of Tyr165 donates a hydrogen to the carbonyl through deprotonation. Concomitantly, NADPH releases a hydrogen from the B-face of the nicotinamide ring onto the susceptible position of the carbonyl group. Thus, the carbonyl group is reduced to an alcohol group, and the isoamyl alcohol and $NADP^+$ are produced. Upon reduction of the carbonyl group, the hydrogen bond between the side chain of Tyr165 and isoamyl alcohol is broken. With the redox state change, the conformation of $NADP^+$ also may change, accompanied by the opening of the interdomain cleft for the release of the product.

4. Conclusions

This work reports the structures of Gre2 and the Gre2–NADPH complex, and reveals a noticeable induced fit upon NADPH binding. These findings provide structural insights into the coenzyme-induced conformational changes of the SDR enzyme for the first time. Computational simulation combined with site-directed mutagenesis and enzymatic activity assays enable us to define the potential substrate-binding site of Gre2. The relatively hydrophobic and extended substrate-binding pocket is why Gre2 can reduce a number of ketones and aldehydes with various structures.

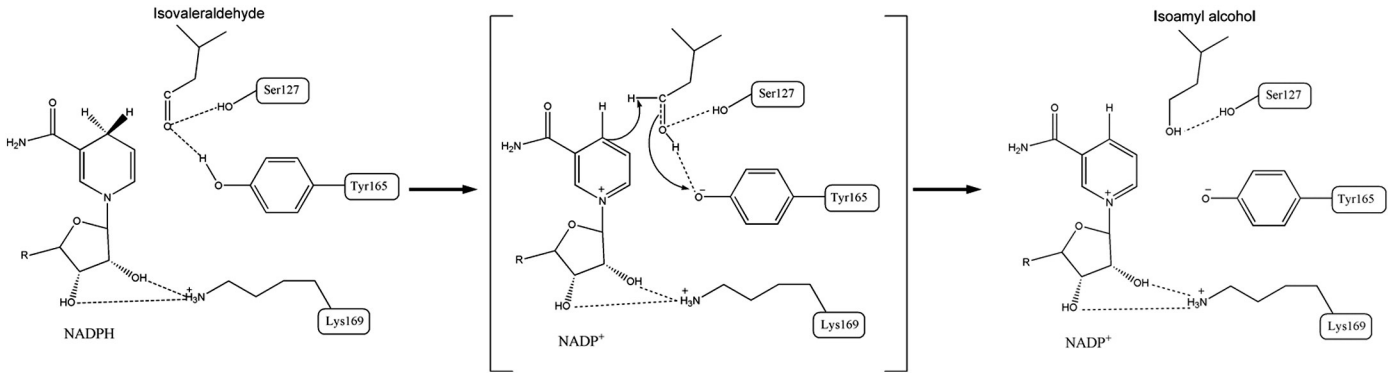

Fig. 5. A scheme showing the catalytic mechanism of Gre2.

5. Accession numbers

The atomic coordinate and structure factor of the Gre2 apo-form and Gre2 complexed with NADPH were deposited in the Protein Data Bank (http://www.rcsb.org) under the PDB IDs: 4PVC and 4PVD, respectively.

Supplementary data to this article can be found online at http://dx.doi.org/10.1016/j.bbapap.2014.05.008.

Acknowledgements

We would like to thank Yong-Liang Jiang at USTC for help in revising the manuscript. We thank the staffs at the Shanghai Synchrotron Radiation Facility for the data collection. We are grateful to all the developers of *CCP4* Suit, *ESPript*, *MolProbity* and *PyMOL*. This work was supported by the 973 project from the Ministry of Science and Technology of China (No. 2012CB911000) and the China Postdoctoral Science Foundation (Programs 2013M542245 and 2013M531930).

References

[1] K. Murata, Y. Fukuda, M. Shimosaka, K. Watanabe, T. Saikusa, A. Kimura, Phenotype character of the methylglyoxal resistance gene in *Saccharomyces cerevisiae*: expression in *Escherichia coli* and application to breeding wild-type yeast strains, Appl. Environ. Microbiol. 50 (1985) 1200–1207.
[2] K. Murata, Y. Fukuda, M. Simosaka, K. Watanabe, T. Saikusa, A. Kimura, Metabolism of 2-oxoaldehyde in yeasts. Purification and characterization of NADPH-dependent methylglyoxal-reducing enzyme from *Saccharomyces cerevisiae*, Eur. J. Biochem. 151 (1985) 631–636.
[3] M. Muller, M. Katzberg, M. Bertau, W. Hummel, Highly efficient and stereoselective biosynthesis of (2S,5S)-hexanediol with a dehydrogenase from *Saccharomyces cerevisiae*, Org. Biomol. Chem. 8 (2010) 1540–1550.
[4] U. Oppermann, C. Filling, M. Hult, N. Shafqat, X.Q. Wu, M. Lindh, J. Shafqat, E. Nordling, Y. Kallberg, B. Persson, H. Jornvall, Short-chain dehydrogenases/reductases (SDR): the 2002 update, Chem. Biol. Interact. 143 (2003) 247–253.
[5] N. Tanaka, T. Nonaka, K.T. Nakamura, A. Hara, SDR: structure, mechanism of action, and substrate recognition, Curr. Org. Chem. 5 (2001) 89–111.
[6] Y. Kallberg, U. Oppermann, H. Jornvall, B. Persson, Short-chain dehydrogenases/reductases (SDRs) — coenzyme-based functional assignments in completed genomes, Eur. J. Biochem. 269 (2002) 4409–4417.
[7] K.I. Varughese, M.M. Skinner, J.M. Whiteley, D.A. Matthews, N.H. Xuong, Crystal structure of rat liver dihydropteridine reductase, Proc. Natl. Acad. Sci. U. S. A. 89 (1992) 6080–6084.
[8] Y. Kallberg, U. Oppermann, B. Persson, Classification of the short-chain dehydrogenase/reductase superfamily using hidden Markov models, FEBS J. 277 (2010) 2375–2386.
[9] J.C. Rutherford, A.J. Bird, Metal-responsive transcription factors that regulate iron, zinc, and copper homeostasis in eukaryotic cells, Eukaryot. Cell 3 (2004) 1–13.
[10] A. Garay-Arroyo, A.A. Covarrubias, Three genes whose expression is induced by stress in *Saccharomyces cerevisiae*, Yeast 15 (1999) 879–892.
[11] M. Krantz, B. Nordlander, H. Valadi, M. Johansson, L. Gustafsson, S. Hohmann, Anaerobicity prepares *Saccharomyces cerevisiae* cells for faster adaptation to osmotic shock, Eukaryot. Cell 3 (2004) 1381–1390.
[12] Z.L. Liu, J. Moon, B.J. Andersh, P.J. Slininger, S. Weber, Multiple gene-mediated NAD(P)H-dependent aldehyde reduction is a mechanism of *in situ* detoxification of furfural and 5-hydroxymethylfurfural by *Saccharomyces cerevisiae*, Appl. Microbiol. Biotechnol. 81 (2008) 743–753.
[13] M. Rep, M. Proft, F. Remize, M. Tamas, R. Serrano, J.M. Thevelein, S. Hohmann, The *Saccharomyces cerevisiae* Sko1p transcription factor mediates HOG pathway-dependent osmotic regulation of a set of genes encoding enzymes implicated in protection from oxidative damage, Mol. Microbiol. 40 (2001) 1067–1083.
[14] C.N. Chen, L. Porubleva, G. Shearer, M. Svrakic, L.G. Holden, J.L. Dover, M. Johnston, P. R. Chitnis, D.H. Kohl, Associating protein activities with their genes: rapid identification of a gene encoding a methylglyoxal reductase in the yeast *Saccharomyces cerevisiae*, Yeast 20 (2003) 545–554.
[15] M. Hauser, P. Horn, H. Tournu, N.C. Hauser, J.D. Hoheisel, A.J. Brown, J.R. Dickinson, A transcriptome analysis of isoamyl alcohol-induced filamentation in yeast reveals a novel role for Gre2p as isovaleraldehyde reductase, FEMS Yeast Res. 7 (2007) 84–92.
[16] M. Katzberg, N. Skorupa-Parachin, M.F. Gorwa-Grauslund, M. Bertau, Engineering cofactor preference of ketone reducing biocatalysts: a mutagenesis study on a gamma-diketone reductase from the yeast *Saccharomyces cerevisiae* serving as an example, Int. J. Mol. Sci. 11 (2010) 1735–1758.
[17] Y.H. Choi, H.J. Choi, D. Kim, K.N. Uhm, H.K. Kim, Asymmetric synthesis of (S)-3-chloro-1-phenyl-1-propanol using *Saccharomyces cerevisiae* reductase with high enantioselectivity, Appl. Microbiol. Biotechnol. 87 (2010) 185–193.
[18] K. Breicha, M. Muller, W. Hummel, K. Niefind, Crystallization and preliminary crystallographic analysis of Gre2p, an NADP(+)-dependent alcohol dehydrogenase from *Saccharomyces cerevisiae*, Acta Crystallogr. Sect. F: Struct. Biol. Cryst. Commun. 66 (2010) 838–841.
[19] Z. Otwinowski, W. Minor, Processing of X-ray diffraction data collected in oscillation mode, Macromol. Crystallogr. A 276 (1997) 307–326.
[20] A. Vagin, A. Teplyakov, Molecular replacement with MOLREP, Acta Crystallogr. D Biol. Crystallogr. 66 (2010) 22–25.
[21] G.N. Murshudov, A.A. Vagin, E.J. Dodson, REFMAC—refinement of macromolecular structures by the maximum-likelihood method, Acta Crystallogr. D Biol. Crystallogr. 53 (1997) 240–255.
[22] P. Emsley, K. Cowtan, Coot: model-building tools for molecular graphics, Acta Crystallogr. D Biol. Crystallogr. 60 (2004) 2126–2132.
[23] I.W. Davis, A. Leaver-Fay, V.B. Chen, J.N. Block, G.J. Kapral, X. Wang, L.W. Murray, W. B. Arendall, J. Snoeyink, J.S. Richardson, D.C. Richardson, MolProbity: all-atom contacts and structure validation for proteins and nucleic acids, Nucleic Acids Res. 35 (2007) W375–W383.
[24] W. DeLano, The PyMOL Molecular Graphics System, DeLano Scientific, San Carlos, CA, USA, 2002. (2002).
[25] P.D. Adams, R.W. Grosse-Kunstleve, L.W. Hung, T.R. Ioerger, A.J. McCoy, N.W. Moriarty, R.J. Read, J.C. Sacchettini, N.K. Sauter, T.C. Terwilliger, PHENIX: building new software for automated crystallographic structure determination, Acta Crystallogr. D Biol. Crystallogr. 58 (2002) 1948–1954.
[26] S.J. de Vries, M. van Dijk, A.M. Bonvin, The HADDOCK web server for data-driven biomolecular docking, Nat. Protoc. 5 (2010) 883–897.
[27] E. Krissinel, K. Henrick, Inference of macromolecular assemblies from crystalline state, J. Mol. Biol. 372 (2007) 774–797.
[28] S.T. Rao, M.G. Rossmann, Comparison of super-secondary structures in proteins, J. Mol. Biol. 76 (1973) 241–256.
[29] S. Kamitori, A. Iguchi, A. Ohtaki, M. Yamada, K. Kita, X-ray structures of NADPH-dependent carbonyl reductase from *Sporobolomyces salmonicolor* provide insights into stereoselective reductions of carbonyl compounds, J. Mol. Biol. 352 (2005) 551–558.
[30] H. Shao, R.A. Dixon, X. Wang, Crystal structure of vestitone reductase from alfalfa (*Medicago sativa* L.), J. Mol. Biol. 369 (2007) 265–276.
[31] N. Trabelsi, P. Petit, C. Manigand, B. Langlois d'Estaintot, T. Granier, J. Chaudiere, B. Gallois, Structural evidence for the inhibition of grape dihydroflavonol 4-reductase by flavonols, Acta Crystallogr. D Biol. Crystallogr. D64 (2008) 883–891.
[32] F. Colonna-Cesari, D. Perahia, M. Karplus, H. Eklund, C.I. Braden, O. Tapia, Interdomain motion in liver alcohol dehydrogenase. Structural and energetic analysis of the hinge bending mode, J. Biol. Chem. 261 (1986) 15273–15280.
[33] H. Eklund, B.V. Plapp, J.P. Samama, C.I. Branden, Binding of substrate in a ternary complex of horse liver alcohol dehydrogenase, J. Biol. Chem. 257 (1982) 14349–14358.
[34] P.C. Guo, X.X. Ma, Z.Z. Bao, J.D. Ma, Y. Chen, C.Z. Zhou, Structural insights into the cofactor-assisted substrate recognition of yeast quinone oxidoreductase Zta1, J. Struct. Biol. 176 (2011) 112–118.
[35] C. Filling, K.D. Berndt, J. Benach, S. Knapp, T. Prozorovski, E. Nordling, R. Ladenstein, H. Jornvall, U. Oppermann, Critical residues for structure and catalysis in short-chain dehydrogenases/reductases, J. Biol. Chem. 277 (2002) 25677–25684.
[36] M.A. Larkin, G. Blackshields, N.P. Brown, R. Chenna, P.A. McGettigan, H. McWilliam, F. Valentin, I.M. Wallace, A. Wilm, R. Lopez, J.D. Thompson, T.J. Gibson, D.G. Higgins, Clustal W and Clustal X version 2.0, Bioinformatics 23 (2007) 2947–2948.
[37] P. Gouet, X. Robert, E. Courcelle, ESPript/ENDscript: extracting and rendering sequence and 3D information from atomic structures of proteins, Nucleic Acids Res. 31 (2003) 3320–3323.